Progress In Electromagnetics Research B, Vol. 54, 1–26, 2013

A MULTI FACETS COMPOSITE PANEL REFLECTARRAY ANTENNA FOR A SPACE CONTOURED BEAM ANTENNA IN KU BAND

Hervé Legay[1, *], Daniele Bresciani[1], Eric Labiole[1], Renaud Chiniard[1], and Raphaël Gillard[2]

[1]Thales Alenia Space Toulouse, 26 Avenue JF Champollion, BP1187, Toulouse Cedex 31037, France

[2]Institut d'Electronique et de Télécommunications de Rennes, UMR CNRS 6164, INSA, 20 av. Des Buttes de Coësmes, Rennes 35043, France

Abstract— A 1.3 m piecewise reflectarray demonstrator has been designed, manufactured and tested, that radiates a contoured beam coverage over North America. A very good agreement is obtained between the theoretical and measured radiation patterns. Many innovative techniques and processes were developed in order to meet the challenging specifications of a space telecommunication antenna.

1. INTRODUCTION

Reflectarray antennas can be an alternative to the traditional shaped reflectors for space contoured beam coverages. They offer very attractive features in terms of manufacturing process: The need for complex shaped moulds is eliminated, and substantial cost and time reductions are expected due to the simplicity and recurring aspects of the reflectarray concept. Besides, many manufacturing steps can be anticipated and the coverage can then be changed at the last moment. In order to be selected as the future generation of contoured beam antennas, the demonstration should be made that reflectarrays can also compete in terms of RF performances with shaped reflectors for typical telecommunication missions. Thus, a study was carried out, that is reported in this paper, with the following objectives: 1) develop the reflectarray technology and the processes; 2) design

Received 14 June 2013, Accepted 1 August 2013, Scheduled 22 August 2013

* Corresponding author: Hervé Legay (herve.legay@thalesaleniaspace.com).

a 1.3 m demonstrator in Ku-Rx band operating in dual polarization; 3) assess the accuracy of the synthesis process, and 4) compare it with that of a shaped reflector antenna.

A contoured beam reflectarray for space applications was first reported in [1]. Later, a reflectarray antenna with two independent beams in dual polarization was developed [2], fulfilling gain requirements over 10% bandwidth. The bandwidth enlargement was achieved with three stacked patches elements, combining the resonances of each patch to offer an increased linearity of the phase-frequency response. However, the resulting three-layer sandwich panel induced manufacturing drawbacks: additional fabrication complexity, increased weight, and high sensitivity to thermo-elastic distortions. Such a panel assembly is therefore not suitable for the harsh space environment.

Alternative methods to increase the bandwidth were then identified, that are suitable for a reflectarray made of a single layer panel. Keeping multiple resonances elements is a necessity, which is achieved either with multiple cross loop elements [3], or with combined patch/slot elements [4]. Reducing the reflectarray lattice is also beneficial for the bandwidth. This has been highlighted by several benchmarking campaigns, either performed by the authors [5], or by Pozar who also considered sub-wavelength elements [6]. For very small lattices, the bandwidth is greatly increased, but at the expense of a lower maximal gain. The gain reduction is due to the fact that the full 360° phase shift range cannot be achieved with single patch elements. In Section 2, we present a novel reflectarray element, derived from the Phoenix element of [7] based on two complementary resonances. It offers an increased linearity of the phase-frequency response and enables a full phase control over the 0–360° range with small reflectarray lattices.

Another factor limiting the bandwidth, which is particularly restrictive in the case of large-sized reflectarrays, is the large range of path lengths between the feed and the reflectarray elements. These path delays must be compensated for over the frequency range by the reflectarray elements. This was done particularly in [2], by adjusting the dimensions of the three-layer printed reflectarray. However, the path delay Δ_{elt} emulated by a reflectarray element Φ_{elt} is related to the variation of the phase with frequency [8], according to:

$$\Delta_{elt} = \frac{\lambda f_0}{2\pi} \frac{\partial \phi_{elt}}{\partial f} \tag{1}$$

where λ refers to the wavelength, and f_0 is the central frequency.

The longer the path delay, the more resonant the element, and the higher the losses, according to the relationship between the resonance

of a reflectarray element and its losses [9, 10]. This correlation was also established experimentally for a number of reflectarray elements etched on various substrates and on a single layer composite panel [11]. The results are summarized in Table 1. In order to prevent losses greater than 0.6 dB, it was recommended to avoid a phase shift variation with frequency greater than 100°/GHz in Ku band, with an objective to maintain it below 60°/GHz. Moreover, keeping the phase variation low with frequency preserves the linearity of the phase shifting elements over a large bandwidth.

Charts provided in [11] indicates that the requested phase variation with frequency reaches 120°/GHz for a typical 1.3 m flat reflectarray, with a focal length of 1.5 m. With a facetted reflectarray, made of panels arranged along a parabolic profile, the requested phase variation with frequency is dramatically decreased, and maintained below 30°/GHz. Faceting the reflectarray will therefore permit to achieve lower losses and larger bandwidth.

Table 1. Measured losses (in dB) at 14.25 GHz for various reflectarray patch elements on thin suspended substrates (with a 4 mm separation with the ground plane) or on a composite panel.

Phase variation with frequency (°/GHz)	Equivalent path delay (in mm)	Measured losses (dB)		
		Substrate 1 $H = 127\,\mu m$, $\varepsilon_r = 2.2$, $\mathrm{Tan}\delta = 0.002$	Substrate 2 $H = 25\,\mu m$, $\varepsilon_r = 3.7$ $\mathrm{Tan}\delta = 0.01$	Panel Assembly (see Figure 3(a))
		0.14	0.1	0.2
−20	17	0.18	0.15	0.35
−40	33	0.25	0.2	0.5
−70	50	0.3	0.3	0.7

The concept of a piecewise planar parabolic reflectarray was initially proposed in [12] mainly for its easiness to be folded. It was implemented for a Space Borne Radar Altimeter [13], with facets along one axis. Its interest in stabilizing the radiation pattern over a frequency band was demonstrated for a SAR antenna [14].

A reflectarray has many more geometrical degrees of freedom than the shaped reflector. Can this advantage be converted into higher performances? A blind optimization of these geometrical parameters is likely to result in sub trapping solutions. Some insight must then be injected in the synthesis process. The conventional approach for

the design of a contoured beam reflectarrays is based on a popular phase-only optimization technique [2, 15]. In Section 3, we present an updated technique that manipulates 2×2 scattering matrices instead of phase. The method has been used for the synthesis of the demonstrator with low cross polarization. By monitoring the polarization response of the reflectarray cells, the cross polarization isolation of the antenna may be improved. This is an example of the possible added value of the reflectarray antenna as compared to the shaped reflector.

Finally, meeting stringent RF requirements with a reflectarray antenna requires a very accurate analysis tool. There are various factors that contribute to small errors in the analysis: the convergence errors of the modeling tool, which were evaluated and reduced as much as possible in [16] for a typical Method of Moment formulation, and mostly the local periodicity assumption, that considers each reflectarray element surrounded by an infinite array of identical elements. In practice, the element dimensions vary smoothly from one cell to the adjacent cells. The approximation is usually considered acceptable for directive beams, and for small antennas, below 20 wavelengths (λ) in size. But what about an antenna with a stringent contoured beam coverage, that is much more sensitive to random phase errors of the electrical field over the radiating aperture? So far, to the knowledge of the authors, only comparisons of simulated and measured contoured beams have been presented [2, 17, 18]. They are claimed satisfactory, but small discrepancies can be seen, which may result locally in gain errors, and particularly at the edge of coverage. Currently, no indicator has been derived in order to assess the uncertainty of the analysis tool, and to compare it with that of a shaped reflector. In Section 5, we propose a white noise model that accounts for it. The model has been identified for the developed demonstrator. It uses a post processing technique that reconstructs the scattering matrices of the reflectarray elements from the measured radiation patterns, compares it then to the simulated ones, and performs a statistic analysis of the differences between them.

2. THE PHOENIX ELEMENT

2.1. Effect of Strong Transitions in the Reflectarray Layout

The local periodicity assumption is particularly violated at the place of sharp transitions within the reflectarray layout. These transitions usually occur when the reflected phase is required to jump after a complete 360 degrees cycle. It has been shown in [19] that such transitions can be responsible for degradations in the array pattern, and should be accounted for in the analysis. In order to have a clear

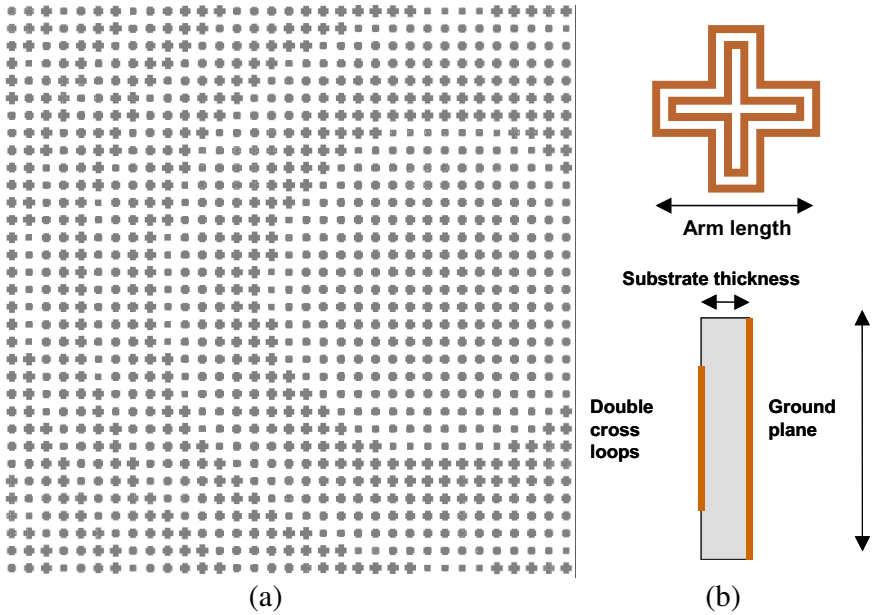

Figure 1. (a) Layout of a reflectarray breadboard made of pharmacist cross elements indicating contours of sharp transitions [3]; (b) detail of the pharmacist cross element.

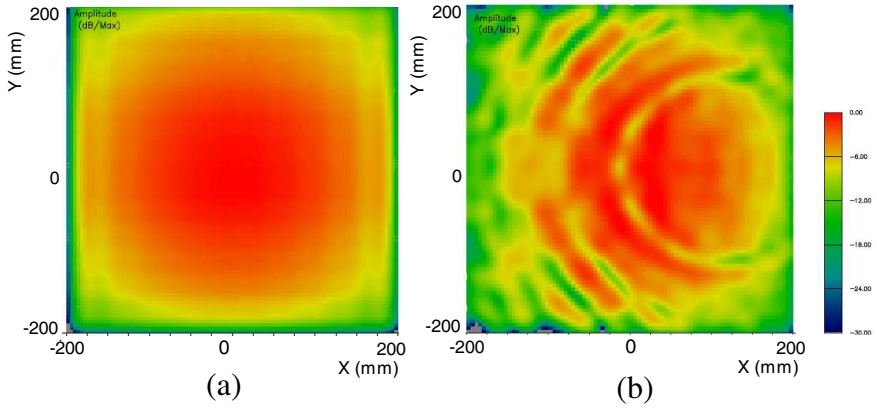

Figure 2. (a) Magnitude (dB/max) of the incident field over the aperture, from simulations; (b) magnitude (dB/max) of the near field measured on the reflectarray surface.

insight, the near field of a reflectarray breadboard made of concentric ring elements with a $0.5\,\lambda$ spacing [3] was measured, Figure 1. With such a dense lattice, the mutual coupling between the elements is strong, and is accounted for quite accurately in the modeling, except for elements close to sharp transitions.

The magnitude of the measured electrical field on the reflectarray surface was compared to that of the illuminated field, Figure 2. It shows that the tapered field distribution induced by the feed is modulated with circular lines on which the electrical field vanishes. These lines correspond to strong transitions between the reflectarray elements, which can be seen in the reflectarray picture, Figure 1. This modulation is responsible for a limited enhancement of the side lobes. It is not a major concern for a small directive beam reflectarray, but may be more problematic for a large size contoured beam antenna.

2.2. The Reflectarray Element with Rebirth Capability

In order to avoid such sudden ruptures of the periodicity of the reflectarray layout, a new generation of reflectarray elements was devised, that ensures a regular and limited progression of the elements parameters from an element to the other, and also provides the unique property to start and end the phase shift cycle with the same element. Such reflectarrays elements are referred to as Phoenix elements. As the Phoenix bird, they reinitialize after a complete life cycle. Consequently, a reflectarray layout made with such Phoenix elements does not exhibit sharp transitions, removing the associated parasitic EM scattering. All the elements operate in quasi periodic conditions.

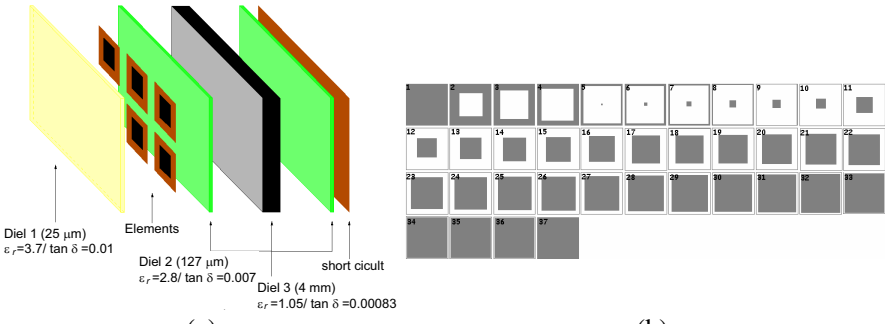

Figure 3. (a) Composite panel, (b) cycle of 37 Phoenix elements. One element is shown every 10°. Only the upper side of the elements is shown. Reflectarray lattice = 10.52 mm ($0.5\,\lambda$ at 14.25 GHz).

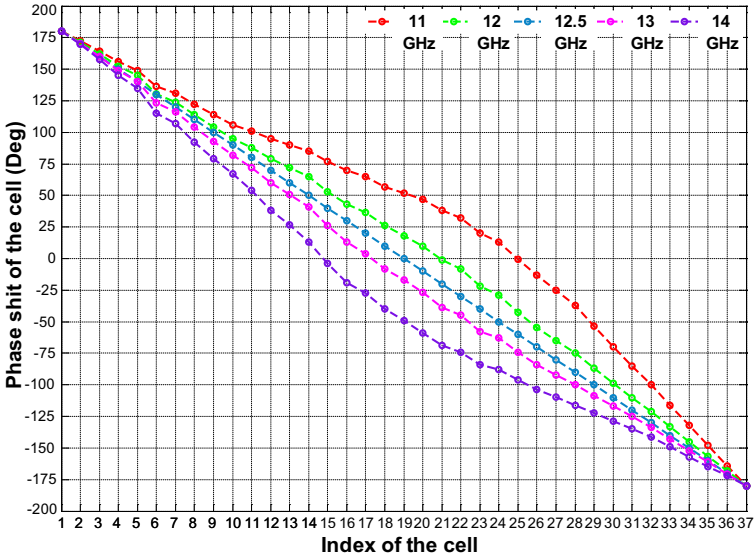

Figure 4. Phase shift variation achieved by a cycle of 37 Phoenix elements at various frequencies (11 GHz, 12 GHz, 12.5 GHz, 13 GHz, 14 GHz).

An initial version of the Phoenix element was presented in [7]. It is based either on a single slotted annular rings or on dual slotted annular rings. This first generation of Phoenix elements enforced a regular phase progression simultaneously with a constant phase dispersion with frequency (approximately 30°/GHz). A simplified library of Phoenix element was used for the demonstrator, which is presented in Figure 3. It starts with a fully metallized cell, achieving 180° over an infinite bandwidth. It then includes some cells with a square aperture of growing size. The aperture is then filled by growing an internal patch, ending with the fully metallized element. The associated phase responses are shown between 11 and 14 GHz, Figure 4.

This new library does not enforce an equal phase shift variation with frequency for all Phoenix elements. It prioritizes low loss and the largest achievable bandwidth. The highest phase variation is 30°/GHz, similar to [7] for the Phoenix element providing a 0° phase shift. For the other elements of the library, a lower phase shift variation is achieved, down to 0°/GHz, and according to Table 1, lower losses are provided. Their phase variation is also linear over a larger bandwidth. Let us explain these attractive features. The Phoenix elements operate with complementary shunt and series LC resonances. The elements of

the library with an intrinsic shunt resonance are said to be inductive (roughly elements 1 to 10 in Figure 3(b), that cover the phase range between 180° to 80°); the elements of the library with an intrinsic series resonance are said to be capacitive (roughly elements 11 to 36 in Figure 3(b), that cover the phase range between 80° to −180°). The 360° phase shift range is thus split in two parts that are covered by two complementary resonances. As a consequence, both resonances are limited to a reduced phase shift range. They can thus be significantly softened, lowering as well the losses.

The various dispersion with frequency of the elements of the library induces a maximum ±7° phase error at the side frequencies of the Ku-Rx bandwidth, that could be even used as a benefit in the design process. For a mission covering a larger bandwidth, such as the whole Ku band, a 2D library of Phoenix elements shall be implemented, that enable an independent control on phase and on phase variation with frequency. Such a library was recently developed [20].

3. THE SYNTHESIS PROCESS

A synthesis process had been developed, that includes two steps: a preliminary synthesis, often referred to as a Phase Only Synthesis (POS), and An advanced Synthesis (AS). The synthesis strategy was presented in detail in [21]. The POS derives a distribution of phase shifts that is easily converted into a layout, through the interpolation of pre-calculated scattering matrices of the Phoenix elements stored in a pre-calculated database computed for different frequencies as well as for different incidence angles. For the calculation of the database, an internal code MIX4 was used, that is based on a mode-matching method between the free space Floquet's modes and the aperture or patch modes of the single cell elements [22]. This code is very efficient in terms of CPU time. It had been widely validated by means of measurements and comparisons with full wave commercial codes.

The second part of the synthesis process, referred to as the advanced synthesis, is more innovative. It is more detailed here-after. It uses as a benefit the fact that the reflectarray phase shifter elements can also slightly depolarize the impinging wave. The cross polarization may therefore be controlled at the level of each element, so that their summated contribution in the radiation pattern is cancelled. This method addresses the cancellation of the total cross-polarized field, in contrast with the methods presented in [23, 24], that are based on a sequential arrangement of cross coefficients in phase opposition, that contribute more to scatter the remaining cross polarization field outside the reflectarray coverage.

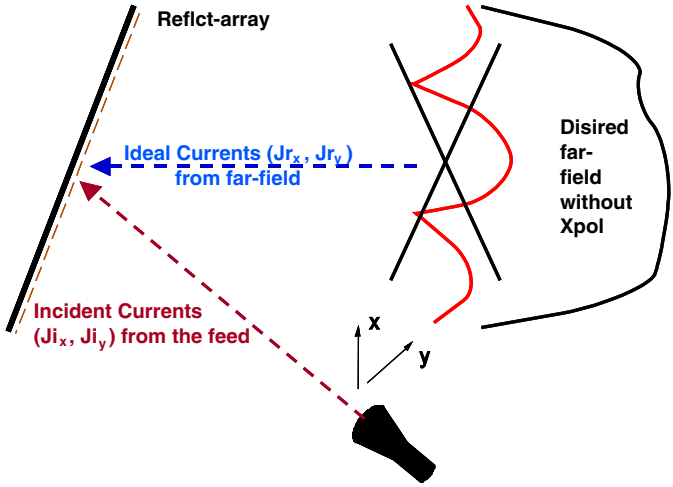

Figure 5. Step 1 of the advanced synthesis: Deriving the scattering matrices of the elements.

3.1. The Theoretical Step of the Advanced Synthesis

The advanced synthesis (AS) starts from the radiation pattern obtained by the preliminary synthesis step. As illustrated in Figure 5, null cross-polarization and equal radiation patterns for the two polarizations are enforced. Currents J_r generating these radiation patterns are reconstructed on the reflectarray surface thanks to back propagation technique. Similarly, the currents J_i corresponding to the illumination feed are also calculated. From these currents, the four reflection coefficients (2×2 scattering matrix) are derived for each reflective cell.

$$\begin{bmatrix} Jr_x \\ Jr_y \end{bmatrix} = \begin{bmatrix} S_{xx} & S_{xy} \\ S_{yx} & S_{yy} \end{bmatrix} \begin{bmatrix} Ji_x \\ Ji_y \end{bmatrix} \tag{2}$$

The observation of the targeted scattering matrices derived from the AS reveals that the co-polarized terms are the same as using the POS. The cross-polarized coefficients that were undergone with the POS, are then controlled with the AS. They usually present a magnitude increase and phase differences between them. Moreover, the energy conservation principle of lossless cells is usually met if the advanced synthesis is adequately linked with the POS synthesis, i.e., if the radiation patterns considered as input parameters of the AS are consistent with the reflectarray geometry.

3.2. Theoretical Advanced Synthesis of a Stringent Coverage over North America with a Facetted Reflectarray

The advanced synthesis was then applied to a 1.3 m reflectarray antenna facetted in five panels. The orientation of the panels was adjusted in order to approach the parabolic shape. The central panel was made as large as possible to avoid transitions in the area strongly illuminated by the feed. The geometry of the antenna is shown in Figure 6, as well as the axes used to define the polarization. The specifications of a Ku-Rx Earth Deck contoured beam telecommunication antenna were considered.

A stringent contoured beam coverage over North America was selected. It includes a large Conus contoured beam with two separate beams over Puerto Rico and Hawaii. This coverage is very sensitive to errors in the elements response. A POS synthesis, followed by the theoretical step of the advanced synthesis were then run, as well as a synthesis of a shaped reflector antenna with the similar main parameter (focal length, diameter, ...). The simulated coverage obtained at the theoretical step of the advanced synthesis is shown at central frequency, Figure 7.

The worst case gain and cross polarization over the four regions of the coverage are reported in Table 2, at the two steps of the synthesis process. The cross polarization of the reflectarray simulated at the POS stage is due to the limited focal length of the antenna. The theoretical AS reflectarray shows that the cross polarization vanishes.

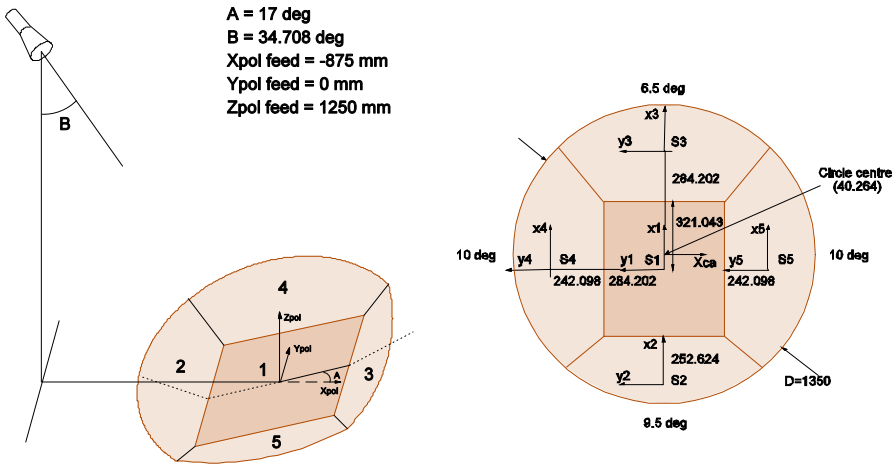

Figure 6. Main dimensions of the reflectarray structure, and panel orientations.

Table 2. Worst case directivity (in dBi) and Cross polarization isolation (dBc) for a contoured beam synthesized with a shaped reflector, a reflectarray (P0S and AS). The same dimensions (focal length, diameter) and the same feed are considered for all cases.

			Conus	**Canada**	**Hawaii**	**Puerto Rico**
Reflectarray — Preliminary Synthesis	H pol	Directivity	29.4	29.5	29.9	29.9
		XPD	25.2	24.1	30.4	35.5
	V-Pol	Directivity	29.5	29.4	29.9	29.8
		XPD	24.1	25.2	30.4	33.6
Reflectarray — Theoretical step of the Advanced Synthesis	H pol	Directivity	29.6	29.6	29.7	30.0
		XPD	42.1	43.6	52.8	53.4
	V-Pol	Directivity	29.5	29.5	29.8	29.8
		XPD	42.1	44.0	52.6	53.3

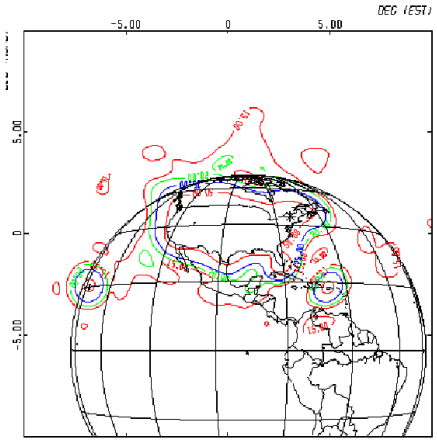

Figure 7. Simulated coverage over Canada, US, Hawaï, Puerto-Rico, at central frequency, 14.25 GHz.

3.3. Layout Synthesis

The second step of the advanced synthesis consisted of deriving the physical layout of each Phoenix element, in order to approach as much as possible the specified scattering matrices. The layout derived at the POS synthesis and based on symmetrical Phoenix elements was considered as the starting point. Then, parallelogram and trapezoid transformations were applied to the reflectarray elements, in order to

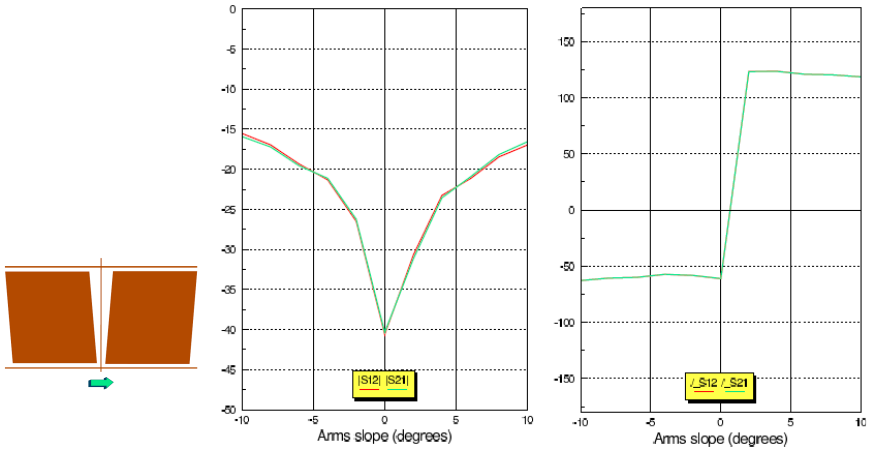

(a) (b)

Figure 8. (a) Range of considered parallelograms with arms slope varying between –10° and 10°; (b) effect of the Parallelogram transformation on the magnitude and phase of the cross polarized components S_{xy} and S_{yx} of the scattering matrices.

achieve the desired cross-coefficients without changing the co-polar ones. The suggested strategy described in [21] was followed. The parallelogram transformation that consists of tilting two opposite sides of the square patch by the same angle, is first applied to provide control on the cross-terms magnitude, as shown in Figure 8. The tilting direction is selected from the phase difference that is requested between the cross coefficients.

By contrast, the trapezoid transformation produces phase differences between the cross-terms, Figure 9. It is based on tilting two opposite sides of the square patch with opposite angles, while preserving also the general original patch size. The trapezoid transformation has little effect on the magnitude of the cross polarization coefficients of the scattering matrices. More details are available in [25] on the transformations and on the design strategies.

The method had been applied to the facetted reflectarray demonstrator, as can be seen on Figure 10. However, the convergence of the iterative procedure was completed for only 30% of the 15000 reflectarray elements. In order to be compatible within reasonable time frame, a smart process driving the iterative procedure needs to be developed. We decided to launch the manufacturing before having totally solved this issue.

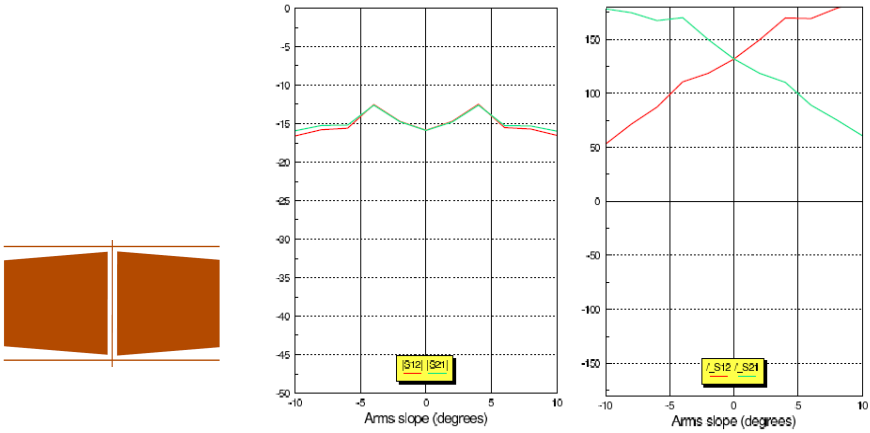

(a) (b)

Figure 9. (a) Range of considered trapezoids with arms slope varying between $-10°$ and $10°$; (b) effect of the Trapezoid transformation on the magnitude and phase of the cross polarized components S_{xy} and S_{yx} of the scattering matrices.

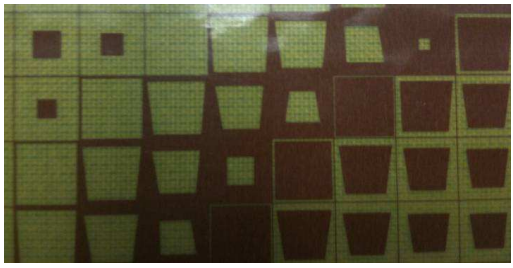

Figure 10. Examples of reflectarray cells that have successfully been transformed in parallelogram/trapezoid.

4. THE FACETTED REFLECTARRAY DEMONSTRATOR

4.1. The Reflectarray Panel

The reflectarray panel has only two partially metallic layers, one for the patch element of variable size, and the second for the ground plane. Such layers are made with thin etched copper cladded substrates separated by transparent honeycomb and stiffening layers. This two-layer panel topology facilitates much the thermal management and the

industrialization process compared to a multi layered panel.

Two samples 880*440 mm^2 have been manufactured and tested in Thermo-Elastic Distortion. The deformations of those large samples at maximum thermal amplitude remained acceptable for Ku applications: less or equal to 100 microns during 2 tests at $-170°C$. The RF panels have also been successfully submitted to a large number of thermal cycling in the range of antennas qualifications $[-180; +165]°C$. The PIM (Passive Inter Modulation Products) tests have also been successfully performed for a set of reflectarray samples.

4.2. The Assembled Reflectarray Antenna

The 1.3 m reflectarray was assembled, Figure 11. Each RF panel was manufactured, and mounted on a CFRP (Carbon Fiber Reinforced Polymer) panel with a sliding junction for the management of the CTE (Coefficient of Thermal Expansion) mismatch. Each panel was positioned on three feet, with a precise shimming. The feed assembly is composed of a dual polarization corrugated horn, a circular-to-square waveguide transition, and a rectangular access. The transition is hand rotated (90°) to switch polarization. The corrugated horn was then mounted on the overall structure made with a conventional metallic technology. Then a 3D control was performed in order to acquire the precise positions of the panels with regard to the feed in order to be able to define the precise shimming for the alignment.

Figure 11. The 1.3 m assembled reflectarray made of five inclined panels.

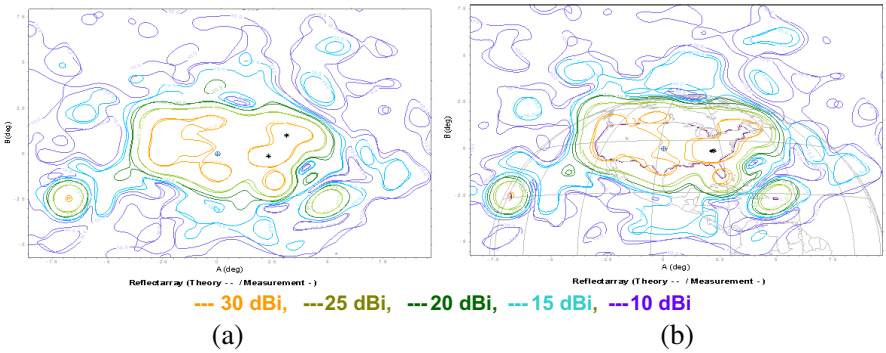

(a) (b)

Figure 12. Comparison of the simulated (dotted lines) and measured (plain lines) radiation patterns (a) in polarization X and (b) in polarization Y, 14.25 GHz.

5. RF MEASUREMENTS OF THE DEMONSTRATOR

5.1. Radiation Patterns

The comparison between simulated and measured radiation patterns is presented for both polarizations at central frequency, either on a contoured plot, Figure 12, or along two representative cuts, Figure 13. The simulated radiation patterns account for the real surface profile of the antenna. The beams over the US, Canada and the narrow beams over Hawaii and Puerto Rico are perfectly positioned for the beam with polarization X. The comparison between the theory and measured radiation patterns indicated a slight ripple, limited to 0.2 dB for the most part of the coverage, and with a worst case of 1.5 dB.

The gain was measured at different locations of the coverage. The measured gain and the cross polarization isolation are also reported in Table 3 and Table 4 for stations scattered all over the coverage. These results indicate that the gain is stable within the 14–14.5 GHz frequency band. The stable variation of the gain within the Ku-Rx band is due to the facetted shape of the reflectarray, which enables the use of 1D library of Phoenix elements presented in Section 2.2.

The gain specification of 28.4 dBi, corresponding to the performances requested for an equivalent shaped reflector, is met for 85% of the cities scattered in the coverage over the Ku-Rx band. The reflectarray antenna exhibits good performances, but is still below the shaped reflector. The cross polarization isolation was measured low, and much below the expected value, with an average value around 25 dBc, and maximal value up to 20 dBc. Once again, the cross polarization isolation improves significantly in the highest part of the

band.

The ohmic losses in the reflectarray panel were derived by comparing the directivity and the gain. They are presented in Table 5 over an extended bandwidth (13.5–15 GHz). They vary between 0.2 and 0.5 dB in the Ku-Rx band, and are slightly higher for polarization X. A significant increase is also noticed at 13.5 GHz, which is interpreted in Section 5.2.

Table 3. Measured gain over the stations of the coverage — polarization X.

	14 GHz		**14.25 GHz**		**14.5 GHz**	
Station	**Gain (dBi)**	**XPD (dBc)**	**Gain (dBi)**	**XPD (dBc)**	**Gain (dBi)**	**XPD (dBc)**
Anchorage	29	23.9	29.2	27.3	29.4	29.7
Atlanta	31.1	21.5	31.4	22.6	31.6	24.1
Boston	31.5	23.9	31.6	24.9	31.4	26.2
Bethel	28.4	24.9	28.5	27.0	28.4	28.6
Chicago	28.2	24.1	28.2	24.4	28.3	25.7
Denver	30	33.7	30.4	32.9	30.5	34.1
Edmonton	29.7	22.3	30.2	24.8	30.3	26.8
Fairbanks	28	21.4	28.1	24.6	28.2	26.4
Halifax	30.5	27.3	30.7	32.9	30.7	36.8
Honolulu	29.7	23.6	30.0	25.3	29.9	25.3
Houston	30.7	21.4	31.0	23.6	31.0	26.5
Juneau	30.1	23.7	30.1	26.1	30.3	29.4
Ketchikan	30.6	24.2	30.9	25.9	31.1	28.5
LA	31	27.5	31.2	29.5	31.3	31.8
Miami	31.6	24.8	31.8	25.9	31.7	27.5
Mineapolis	28.1	20.7	27.9	21.9	27.8	23.1
Montreal	32.5	30.8	32.6	29.8	32.5	30.7
NY	31.7	23.4	31.6	24.5	31.3	25.0
Quebec	32.4	33.8	32.5	33.2	32.3	35.0
SF	30.6	33.0	31.0	34.3	31.2	34.9
SJn	29.5	31.2	29.6	33.1	29.1	36.4
Seattle	30.9	24.9	31.3	25.0	31.7	26.6
Toronto	30.3	24.6	30.6	24.8	30.6	25.3
Vancouver	31.1	23.8	31.4	24.2	30.6	25.9
Winnipeg	29.4	21.3	29.6	22.7	29.6	24.8

Table 4. Measured gain over the stations of the coverage — Polarization Y.

Station	14 GHz		14.25 GHz		14.5 GHz	
	Gain (dBi)	XPD (dBc)	Gain (dBi)	XPD (dBc)	Gain (dBi)	XPD (dBc)
Anchorage	28.8	19.6	29.0	20.5	29.3	22.0
Atlanta	31.9	26.0	32.1	26.1	32.1	26.8
Boston	31.0	27.7	30.9	30.6	31.0	32.9
Bethel	28.3	22.4	28.3	23.3	28.3	24.6
Chicago	29.5	26.6	29.5	26.9	29.5	26.7
Denver	31.4	29.6	31.5	29.3	31.5	30.0
Edmonton	29.8	23.6	30.1	24.6	30.3	26.7
Fairbanks	27.5	18.7	27.7	19.3	28.0	20.4
Halifax	30.3	34.1	30.5	35.6	30.6	35.3
Honolulu	29.4	22.8	29.8	24.4	30.0	24.9
Houston	30.6	25.1	30.8	26.1	30.9	26.6
Juneau	29.3	21.6	29.8	22.5	30.1	23.9
Ketchikan	30.2	24.1	30.5	24.9	30.8	26.2
LA	28.1	32.6	28.0	30.9	27.9	30.2
Miami	31.3	31.9	31.5	33.3	31.9	36.5
Mineapolis	28.8	23.5	30.2	25.0	31.2	27.1
Montreal	28.2	31.2	28.0	30.8	27.9	31.0
NY	32.0	26.5	32.1	28.5	32.0	31.0
Quebec	31.2	27.5	31.0	27.7	30.8	28.3
SF	30.6	29.5	31.0	29.2	31.2	28.8
SJn	31.5	30.4	31.8	32.4	32.0	33.3
Seattle	29.6	28.9	29.5	30.5	29.2	33.5
Toronto	30.9	26.1	30.6	27.4	30.8	31.4
Vancouver	30.2	27.4	31.2	28.7	31.6	31.1
Winnipeg	30.8	27.7	29.9	30.7	30.1	32.0

Table 5. Measured losses (dB) at various frequencies (GHz).

Frequency (GHz)	13.5	13.75	14	14.25	14.5	14.75	15
Polarisation X	0.8	0.7	0.5	0.4	0.3	0.3	0.4
Polarisation Y	0.4	0.4	0.4	0.3	0.2	0.2	0.4

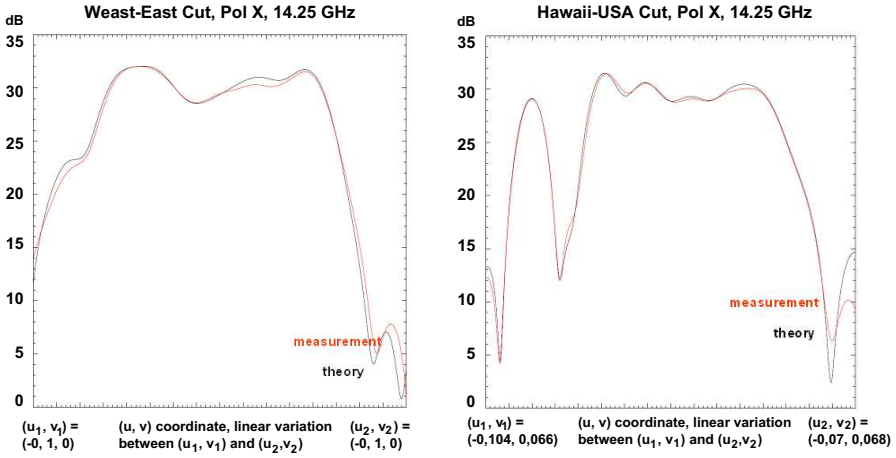

(a)

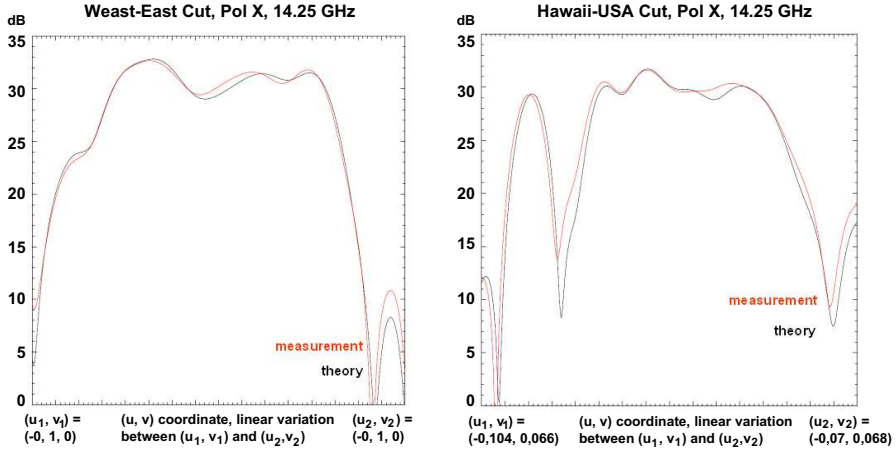

(b)

Figure 13. Comparison of the simulated (black lines) and measured (red lines) radiation patterns (a) in polarization X and (b) in polarization Y, 14.25 GHz. East-West Cuts and a diagonal cut through Hawaii and USA.

5.2. Detection of Wood's Anomalies

RF diagnosis techniques have been proposed to reconstruct the near field over a radiating aperture [26]. The phase shift of the reflectarray elements can thus be reconstructed. A more efficient RF diagnosis tool was developed, that reconstructed the equivalent scattered currents

on the whole reflectarray surface and then the four terms of the real scattering of each reflectarray element. It helps provide a good understanding and characterize the accuracy of the synthesis process.

Similarly to the advanced synthesis process presented in Section 3.1, the tool reconstructs the scattering matrices from the measured radiation patterns in both polarizations, and from the measured radiation pattern of the primary horn. It allowed to detect an unexpected phenomenon: Some reflectarray elements were altered by a sharp resonance centered around 13.5 GHz (outside of the bandwidth) that generated losses. This is more pronounced for the polarization X. The contour of the lossy elements is shown in Figure 14 for the central panel is similar to the contour of the layout. At 14.25 GHz, the losses are much lower. The average loss, around 0.3 dB, is consistent with the ohmic loss derived from the gain measurement.

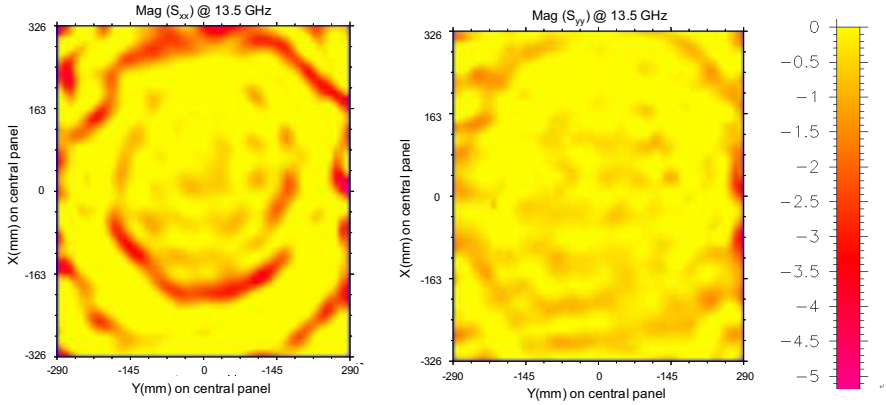

Figure 14. Magnitude of the Co-polarization components S_{xx} and S_{yy} of the scattering matrices of the reflectarray elements of the central panel reconstructed from the measured radiation pattern (13.5 GHz).

An analysis campaign was then carried out with MIX4, the mode matching software used in the analysis of periodic surface, as well as with various EM tools (HFSS, Designer, CST). It confirmed the occurrence of a sharp resonance for a limited number of reflectarray elements. This resonance does not occur for a normal incidence ($\theta = 0°$, $\phi = 0°$). It occurs as soon as θ increases. Losses are induced. For an oblique incidence ($\theta > 0°$, $\phi > 0°$), the resonance generates losses as well as conversion of the energy in the orthogonal polarization, Figure 15. The observed phenomenon corresponds to the so called Wood's anomalies, reported by Wood in 1902 for optical gratings [27]. It deals with the excitation of surface waves if the incident wave excites a Floquet mode whose wave number matches that of a surface wave.

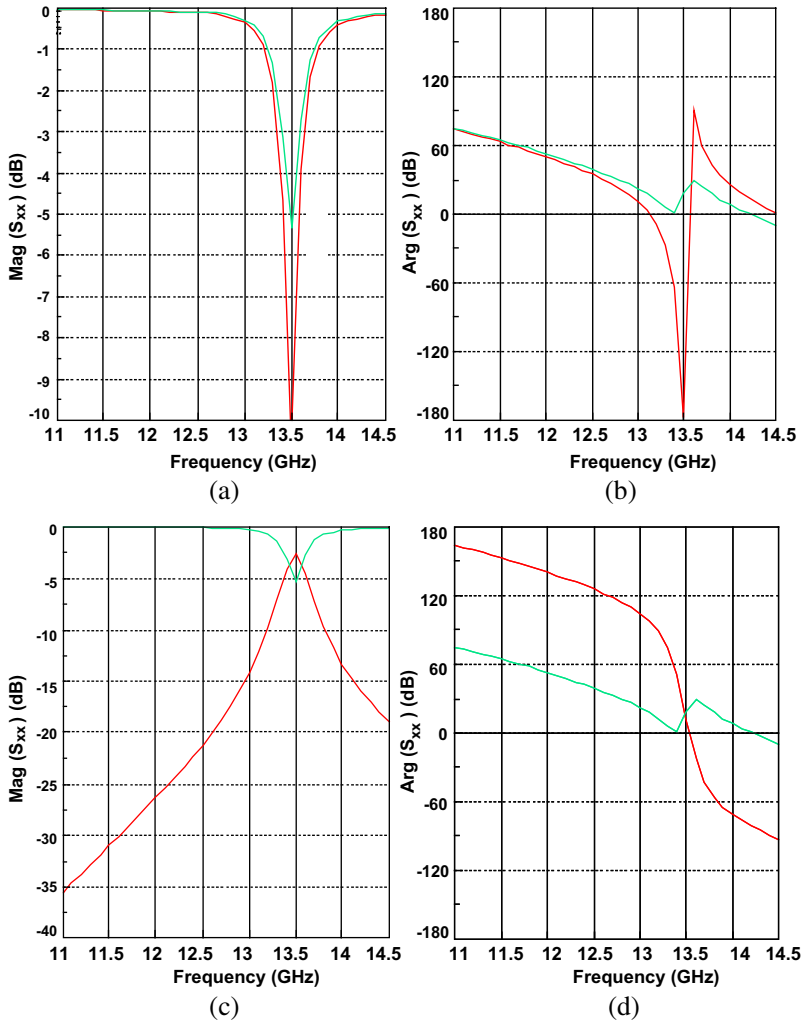

Figure 15. Scattering matrices of a reflectarray elements with a parasitic resonance (a) red: Mag (S_{xx}), green: Mag (S_{xx}), (b) red: Arg (S_{xx}), green: Arg (S_{xx}), (c) red: Mag (S_{xy}), green: Mag (S_{xx}), (d) red : Arg (S_{xy}), green: Arg (S_{xx}).

The matching of the incident plane wave with the substrate wave induces a slight rotation of the polarization of the wave for an oblique incidence. Thus, the diagnosis tool detects an increase of the cross polarization components of the scattering matrices due to this wood's anomaly, as shown in Figure 16 for the central panel of the

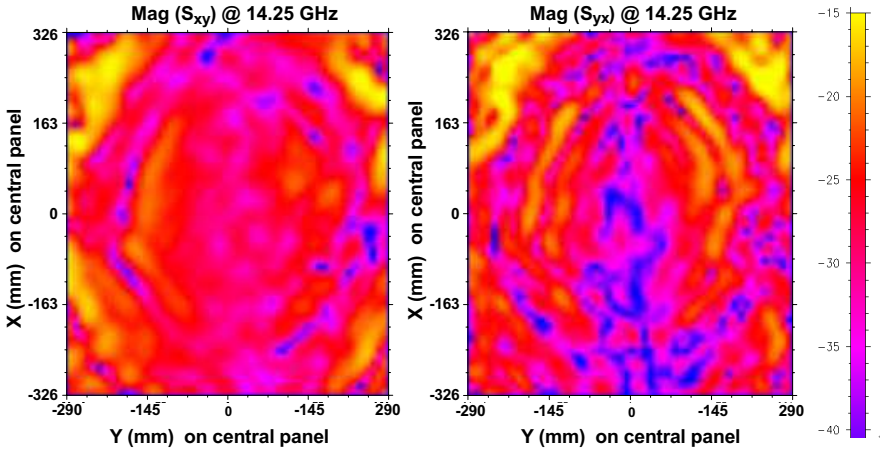

Figure 16. Magnitude of the Cross-polarization components S_{xy} and S_{yx} of the scattering matrices of the reflectarray elements of the central panel reconstructed from the measured radiation pattern (14.25 GHz).

demonstrator. The reflectarray elements located on the upper part of the central panel, and illuminated with high oblique incidence, are mostly concerned with this cross polarization conversion.

It is the first time, to the knowledge of the authors, that Wood's anomalies were identified for reflectarray antennas. Means for circumventing it have been identified but could not be implemented in the frame of this study. These Wood's anomalies are responsible for the too high losses and cross polarization level.

5.3. A RMS Indicator Characterizing the Synthesis Accuracy

Comparing the contours of the theory-experiment radiation patterns is not sufficient to conclude on the accuracy of the synthesis process, since the discrepancies induced on radiation patterns are very coverage dependent. Coverage with moderate shaped beam, usually considered in publications, are relatively robust to phase errors on the radiating aperture. For composite coverage made of a wide beam and directive spots, as in the present paper, the sensitivity of the radiation pattern to the error is high. For this reason, we propose to derive a metric, such as an equivalent RMS, in order to quantify the accuracy of a design process. This indicator could then be used, regardless of the coverage.

This RMS indicator is obtained with the RF diagnosis tool. First, for each reflectarray element, the phases of the co-polarized coefficients

of the simulated and of the reconstructed scattering matrices were compared. The phase difference characterizes the accuracy of the synthesis process. The major contributors are: the manufacturing errors (thickness of the layers, knowledge of the electrical parameters, ...), the accuracy of the analysis tool due to the convergence or to the local periodicity assumption, and the misalignment and the deformation of the panels. For reducing the error related to the analysis, the numerical parameters were set in order to achieve convergence on Wood's anomalies.

The phase errors corresponding to the mechanically measured out of plane deformation and misalignment of the panel were also subtracted. Finally, the distribution of the remaining phase errors were processed and represented an equivalent distortion of the five panels, expressed in mm. The equivalent distortion of the central panel corresponding to the synthesis uncertainty for both polarizations is shown in Figure 17. These errors derived from the measurements in the two polarizations are correlated, and a bit more emphasized for the X polarization. This is mainly due to the wood's anomalies that mostly affect the polarization X. The contours of the errors are very linked with the phase shift distribution achieved on the panel. See the central panel in Figure 11. The errors are also more pronounced for the upper side of the panel, which is also concerned with a more oblique incidence. Wood's anomalies are possible significant factor for

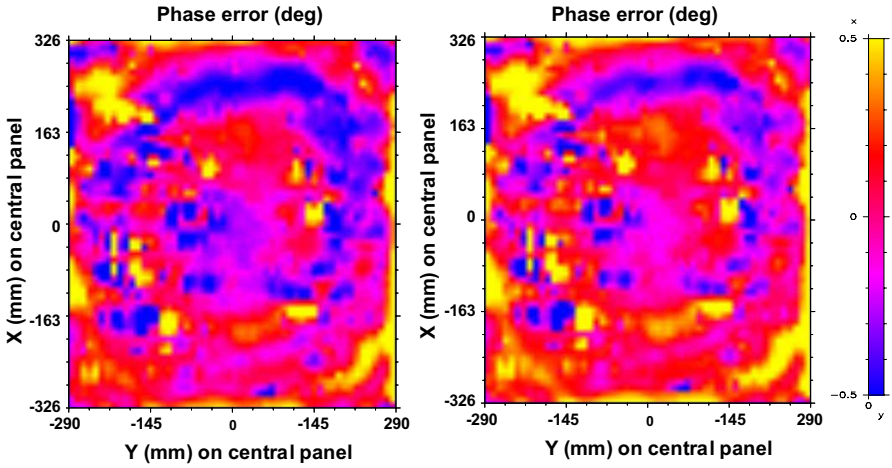

Figure 17. Magnitude of the Cross-polarization components S_{xy} and S_{yx} of the scattering matrices of the reflectarray elements of the central panel reconstructed from the measured radiation pattern (14.25 GHz).

this uncertainty, since they induce some phase variation, as shown in Figure 15(b).

Statistically, over the whole antenna, these errors can be represented as an equivalent RMS shape deviation error estimated respectively at 290 µm and 310 µm for X and Y polarizations. This corresponds to a $\lambda/60$ RMS accuracy. It is still a bit too much for contoured beam with stringent coverages, and explains the slight discrepancies observed between the measured and theoretical radiation patterns. It is expected that removing the Wood's anomalies will help in reducing this RMS accuracy indicator.

6. SUMMARY

Thales Alenia Space and its partners have designed, manufactured and tested a 1.3 m piecewise planar parabolic reflectarray antenna, and have demonstrated the capability for the reflectarray to meet the challenging specifications of a telecommunication antenna. The development included various innovations: A novel reflectarray element was developed that avoids sharp transitions. This element revealed excellent features in terms of bandwidth. An original synthesis method was developed, that allows the analysis of a piecewise planar parabolic reflectarray, and its synthesis with the reduction of the cross-polarization. The technology and the processes were developed, and a 1.3 m reflectarray antenna made of five panels was manufactured and tested. The measurement indicated that some elements were altered by a parasitic resonance, that was so sharp, that the analysis did not forecast. This parasitic resonance distorted the zero cross polarization synthesis. Its detection was allowed thanks to an efficient diagnosis tool. The parasitic resonance was identified as a Wood's anomaly.

The diagnosis tool was used to derive an indicator that characterizes the accuracy of the synthesis process. It is expressed as a RMS shape deviation error. The uncertainty of our synthesis process is equivalent to a $\lambda/60$ RMS surface accuracy. It is still a bit too high for contoured beam antennas for space applications. Ways to decrease this uncertainty had been identified, and are the object of current developments.

ACKNOWLEDGMENT

The authors would like to thank E. Girard, G. Caille, D. Calas, B. Salome from Thales Alenia Space, L. Marnat, R. Loison from IETR, G. Toso, C. Mangenot from ESA-ESTEC, and J. M. Lopez from CNES for providing valuable support.

REFERENCES

1. Pozar, D. M., S. D. Targonski, and R. Pokuls, "A shaped-beam microstrip patch reflectarray," *IEEE Transactions on Antennas and Propagation*, Vol. 47, No. 7, 1167–1173, Jul. 1999.
2. Encinar, J., L. Datashvili; J. Zornoza, M. Arrebola, M. Sierra-Castaner, J. Besada-Sanmartin, H. Baier, and H. Legay, "Dual-polarization dual-coverage reflectarray for space applications," *IEEE Transactions on Antennas and Propagation*, Vol. 54, 2827–2837, Oct. 2006.
3. Chaharmir, M. R., J. Shaker, and H. Legay, "Broadband design of a single layer large reflectarray using multi cross loop elements," *IEEE Transactions on Antennas and Propagation*, Vol. 57, No. 10, 3363–3366, Oct. 2009.
4. Cadoret, D., A. Laisne, R. Gillard, and H. Legay, "A New reflectarray cell using coupled microstrip patches loaded with slots," *Microwave and Optical Technology Letters,* Vol. 44, No. 3, 270–273, Feb. 2005.
5. Legay, H., B. Salome, E. Labiole, M. A. Millon, D. Cadoret, R. Gillard, M. R. Chaharmir, and J. Shaker, "Reflectarrays for satellite telecommunication antennas," *EuCAP 2007*, 1–6, Edinburgh, 2007.
6. Pozar, D., "Wideband Reflectarrays using artificial impedance surface," *Elec. Let.*, Vol. 43, No. 3, 148–149, Feb. 2007.
7. Moustafa, L., R. Gillard, F. Peris, R. Loison, H. Legay, and E. Girard, "The Phoenix cell: A new reflectarray cell with large bandwidth and rebirth capabilities," *IEEE Antennas and Wireless Propagation Letters*, Vol. 10, 71–74, 2011.
8. Huang, J., "Bandwidth study of microstrip reflectarray and a novel phased reflectarray concept," *Antennas and Propagation Society Intl. Symp., AP-S. Digest*, Vol. 1, 582–585, Jun. 1995.
9. Bozzi, M., S. Germani, and L. Perregrini, "A figure of merit for losses in printed reflectarray elements," *IEEE Antennas and Wireless Propagation Letters*, Vol. 3, No. 1, 257–260, 2004.
10. Rajagopalan, H. and Y. Rahmat-Samii, "On the reflection characteristics of a reflectarray element with low-loss and high-loss substrates," *IEEE Antennas and Propagation Magazine*, Vol. 52, No. 4, 73–89, 2010.
11. Legay, H., B. Salome, E. Labiole, M. A. Milon, D. Cadoret, R. Gillard, R. Chaharmir, and J. Shaker, "Reflectarrays for satellite telecommunication antennas," *EuCAP 2007*, 1–6, Edinburgh, Nov. 11–16, 2007.

12. Roederer, A. G., "Reflector antennas in flat panels," US Patent 6411255, filed Mar. 6, 2001.
13. Hodges, R. and M. Zawadzki, "Design of a large dual polarized Ku-band reflectarray for spaceborne radar altimeter," *IEEE AP-S Symposium*, 4356–4359, Monterey, CA, Jun. 2005.
14. Legay, H., B. Salomé, E. Girard, S. Ramongassié, J. Encinar, and G. Toso, "Reflectarrays antennas for SAR missions," *Proc. International Symposium on Antenna Technology and Applied Electromagnetics (ANTEM)*, Saint Malo, Jun. 2005.
15. Bucci, O. M., A. Capozzoli, G. D'Elia, P. Maietta, and S. Russo, "An advanced reflectarray design technique," *Proc. 28th ESA Antenna Workshop*, 68, Noordwijk, The Netherlands, 2005.
16. Zhou, M., E. Jørgensen, O. S. Kim, S. B. Sørensen, P. Meincke, and O. Breinbjerg, "Accurate and efficient analysis of printed reflectarrays with arbitrary elements using higher-order hierarchical Legendre basis functions," *IEEE Antennas and Wireless Propagation Letters*, Vol. 11, 814–817, 2012.
17. Legay, H., D. Bresciani, E. Labiole, R. Chiniard, E. Girard, Q. Guillard, L. Marnat, R. Loison, R. Gillard, and G. Toso, "Reflectarrays for contoured beams antennas in Ku band," *Proc. 32nd ESA Antenna Workshop*, Noordwijk, The Netherlands, 2010.
18. Zhou, M., S. B. Sørensen, E. Jørgensen, P. Meincke, O. S. Kim, and O. Breinbjerg, "Direct optimization of printed reflectarrays for contoured beam satellite antennas applications," *IEEE Transactions on Antennas and Propagation*, Vol. 61, No. 4, 2013.
19. Milon, M. A., D. Cadoret, R. Gillard, and H. Legay, "Surrounded-element approach for the simulation of reflectarray radiating cells," *Microw. Antennas Propag.*, Vol. 1, No. 2, 289–293, Apr. 2007.
20. Legay, H., D. Bresciani, E. Labiole, R. Chiniard, E. Girard, G. Caille, D. Calas, R. Gillard, and G. Toso, "A 1.3 m facetted reflectarray in Ku band," *15th International Symposium on Antenna Technology and Applied Electromagnetics (ANTEM)*, Toulouse, Jun. 2012.
21. Legay, H., D. Bresciani, E. Labiole, R. Chiniard, E. Girard, G. Caille, D. Calas, R. Gillard, and G. Toso, "A 1.3 m earth deck reflectarray for a Ku-band contoured beam antenna," *Proc. 33rd ESA Antenna Workshop*, Noordwijk, The Netherlands, 2011.
22. Bresciani, D., "A unified approach to the characterization of frequency and polarization selective surfaces," *IEEE International Antennas and Propagation Symposium*, Vol. 3, 1960–1963, Ann

Arbor, Michigan, USA, 1993.

23. Hasani, H., M. Kamyab, and A. Mirkamali, "Low cross-polarization reflectarray antenna," *IEEE Transactions on Antennas and Propagation*, Vol. 59, No. 5, 1752–1756, May 2011.
24. Tienda, C., J. Encinar, M. Barba, and M. Arrebola, "Reduction of cross-polarization in offset reflectarrays using two layers of varying sized patches," *Microwave and Optical Technology Letters,* Vol. 54, No. 11, Nov. 2012.
25. Artiga, X., D. Bresciani, H. Legay, and J. Perruisseau-Carrier, "Polarimetric control of reflective metasurfaces," *IEEE Antennas and Wireless Propagation Letters*, Vol. 11, 1489–1492, 2012.
26. Rahmat-Samii, Y., "Microwave holography of large reflector antennas — Simulation algorithms," *IEEE Transactions on Antennas and Propagation*, Vol. 33, No. 11, 1194–1203, Nov. 1985.
27. Wood, R. W., "On the remarkable case of uneven distribution of a light in a diffraction grating spectrum," *Philos. Mag.*, Vol. 4, 396–402, 1902.